Mechanism and Solution of Inaccurate Perturbation Output of DC-AC Type IMU

Peijun Zhong, *Student Member, IEEE*, Jianjun Sun, *Member, IEEE*, Pan Yu, *Student Member, IEEE*, Yi Liu, *Member, IEEE*, and Xiaoming Zha, *Senior Member, IEEE*

***Abstract*—Impedance measurement unit (IMU) with injection of broadband perturbations is widely used to obtain grid and converter impedance. The accuracy of measured impedance and the power quality of the measured system rely on the amplitude control of the injected perturbations. However, the accuracy of output perturbation of IMU is lack of attention especially around the fundamental frequency of the measured system. In this brief, a three-phase DC-AC type IMU is introduced and the mechanism and solution of inaccurate perturbation output of the IMU is study. First, the DC-AC type IMU with PR current controllers, DC voltage controller and phase locked loop (PLL) is introduced. Next, the mechanism of inaccurate perturbation output is analysis, which is caused by the introduction of DC voltage ripple. Then, improved DC voltage control solutions with notch filter or delay filter are proposed to achieve the accurate control of single-frequency and multi-frequency perturbation current respectively. Finally, control hardware-in-the-loop experiment results are given to demonstrate and verify the effectiveness and feasibility of the proposed method.**

***Index Terms*—Impedance measurement, dc-ac type impedance measurement unit, inaccurate perturbation output, improved dc voltage control solutions.**

I. Introduction

MORE power converters are integrated into the power system and railway traction power supply system for their flexible and controllable characteristics [1], [2]. Subsequently, resonances or instability issues occur frequently in the power converters integrated-system [3]. Impedance-based small signal stability analysis method is widely used to explain the stability behavior of grid connected converters [4]. And some control strategy optimization with the knowledge of grid impedance is implanted into power converters controller to improve the adaptability of converters in a weak grid [5]. In recent studies, the impedance is also be used to estimate the nodal inertia and frequency regulation capability of the power source node [6]. Evidently, the impedance of the grid or the grid-tied converter from a few hertz to several thousand hertz is a critical parameter in the above application scenarios. The grid impedance and the grid-tied converter impedance can be obtained by modeling in *dq* or *abc* reference frame [4] with the knowledge of all the parameters and structure of the controller and circuit, which makes it an infeasible solution in the site.

Fortunately, measurement provides another effective way to obtain the impedance of the grid and converter without the detailed parameter and structure information, where the grid or converter are treated as a black-box model. Different forms of perturbation signals are used in measurement, such as the sine signal [7], multi-sine signal [8], impulse signal [9], and pseudo-random binary sequence (PRBS) [10], *etc.* Among these signals, the sine signal and multi-sine signal have the desired signal-to-noise ratio and are attractive signals in actual testing. These signals are converted into perturbations and injected into the measured system by switching equipment, introducing perturbation signals in the existing converter, or accessing an impedance measurement unit (IMU). In [11], the transient impulse signal is injected into the measured system by switching the capacitor or resistive, but the high-frequency components of injected perturbation will decay rapidly and the measurement accuracy is highly limited. The method of introducing perturbation signals into the controller of the existing converter of the measured system has been studied in [9] and [10]. The dilemma is the impedance of the converter itself cannot be measured and the converter bear the risk of over modulation. An IMU should be connected to the measured system to obtain the impedance of both the grid and grid-tied converter and IMUs with different topology types have been studied for impedance measurement. In [12], a butterfly-type disturbance circuit is presented to generate chirp pulse-width modulation signal. And the three phase half-bridge topology [13] is used to generate chirp signal with open control. However, the IMU with open control in [12], [13], is unable to regulate the injection current accurately and may case, which will cause power quality problems due to large current injection, and affect the accurate of impedance measurement results when the injected current is too small and the measured system owns high noise [14], [15].

The cascaded H-bridge topology with closed open is applied in [7], [16], [17], [18], to inject sinusoidal perturbation into the measured system. In general, these devices can achieve perturbation injected and impedance measurement. However, when the frequency of injected perturbation approaches the fundamental frequency of the measured system, the ripple voltage of DC capacitance will affect the accuracy of the generated perturbation. In [18], the influence of the ripple voltage of DC capacitance was mentioned in a H-bridge topology. However, the influence mechanism of DC ripple voltage and detailed solutions have not been introduced. In this brief, a DC-AC type IMU with a three-phase half-bridge topology is used to generated sinusoidal perturbation, and the mechanism and solution of inaccurate perturbation output is presented.

Manuscript received 6 February 2023; revised 14 April 2023; accepted 10 May 2023. Date of publication 15 May 2023; date of current version 30 June 2023. This work was supported by the National Natural Science Foundation of China under Grant 52007136. This brief was recommended by Associate Editor J. Liu. *(Corresponding authors: Jianjun Sun; Pan Yu.)*

The authors are with the School of Electrical Engineering and Automation, Wuhan University, Wuhan 430072, China (e-mail: pjzhong@whu.edu.cn; jjsun@whu.edu.cn; pyu@whu.edu.cn).

Color versions of one or more figures in this article are available at https://doi.org/10.1109/TCSII.2023.3275969.

Digital Object Identifier 10.1109/TCSII.2023.3275969

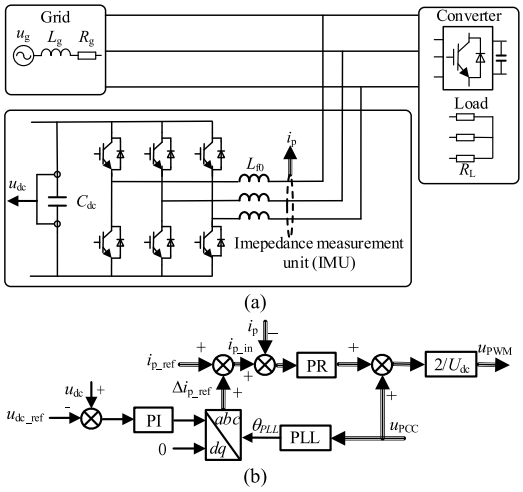

Fig. 1. Example system for impedance measurement demonstration. (a) The measured system diagram. (b) The control strategy of IMU.

The remainder of this brief is organized as follows. The principle of the DC-AC type IMU with a three-phase half-bridge topology is introduced in Section II. In Section III, the mechanism and solution of inaccurate perturbation output of the IMU is analyzed. Results based on control hardware-in-the-loop (CHIL) experiments are shown in Section IV. Section V draws the conclusion.

II. Principle of the DC-AC Type IMU

In the impedance measurement system, a IMU is often connected to the point of common coupling (PCC) and applied to obtain the impedance of the grid, grid-tied converter or load as shown in Fig. 1(a), where the example measured system consists of the grid, grid-tied converter or load and DC-AC type IMU. The IMU employs a conventional three-phase half-bridge topology and the inductance L_f is a filter to prevent switching subharmonics from being injected into the measured system. The DC side capacitor C_{dc} is used to provide voltage support for the IMU during perturbation injection. It should be noted that the DC-AC type IMU is active front end free compared with the device proposed in [17]. However, the introduced IMU is mainly applicable to low-voltage networks such as 380V due to the limitation of IGBT voltage and current stress.

The overall control strategy of the IMU is also shown in Fig. 1(b), where the DC voltage control, phase-locked loop (PLL), current control, and voltage-feedforward control are adopted. The DC voltage control is used to regulate and maintain DC capacitor voltage u_{dc}. The deviation between the actual value u_{dc} and the reference value u_{dc_ref} of DC voltage is processed by a PI controller. The transfer function G_{PI} of the PI controller is given by

$$G_{PI}(s) = k_{pdc} + k_{idc}/s \tag{1}$$

where k_{pdc} and k_{idc} is the proportional coefficient and integral coefficient of the PI controller, respectively.

The PLL is used to detect the phase of PCC voltage u_{PCC} and is implemented by a synchronous reference frame PLL [19]. The detected phase θ_{PLL} is the rotation angle in dq to abc transformation, where the output of the DC voltage control is treated as d-axis component and the q-axis component is 0. The obtained component in abc-axis is Δi_{p_ref}, which can be regarded as an additional current command to maintain DC voltage stability. In the current control loop, the sum of the perturbation current command i_{p_ref} and the additional current command Δi_{p_ref} minus the actual output current and then inputs the difference value into the multi-resonant PR controller, which is represent with one PR module for simplify in Fig. 1(b). The multi-resonant PR controller consists of fundamental PR and perturbation PR controller. The transfer function G_{PR} of multi-PR controller can be expressed as

$$G_{PI}(s) = (k_{p0} + \frac{k_{r0}s}{s^2 + (2\pi f_0)^2}) + \sum_{n=1}^{m} (k_{ppn} + \frac{k_{rpn}s}{s^2 + (\omega_{pn})^2}) \tag{2}$$

where k_{p0} and k_{r0} is the proportional coefficient and resonance coefficient of fundamental PR, and the f_0 is the fundamental frequency of the measured system. The second item of equation (2) is perturbation PR controllers, where m represents the number of each injected perturbation, k_{ppn} and k_{rpn} is the proportional coefficient and resonance coefficient of the n-th perturbation PR controller, and ω_{pn} is the angular frequency of the n-th perturbation.

The last part of the control strategy of the IMU is voltage-feedforward loop, where the PCC voltage u_{PCC} is imposed in the output port of current controller and a proportional link with a gain of $2/U_{dc}$ is implanted into the controller before the modulated signal u_{PWM} is finally generated.

III. The Mechanism and Solution of Inaccurate Perturbation Output

Accurate control of output perturbation of the IMU is an important prerequisite for impedance measurement. However, inaccurate perturbation output of the IMU will appear, accompanied by coupling component, when the injected perturbation frequency is close to the fundamental frequency of the measured system. The mechanism and corresponding solution of inaccurate perturbation output of the IMU will be introduced in this section.

A. Mechanism Analysis

The single-frequency or multi-frequency perturbation components are into the measured system by the IMU during impedance measurement. To simplify the analysis of the mechanism of inaccurate perturbation output, the output perturbation of IMU is assumed to be i_p, which contains only one frequency component. And the PCC voltage u_{PCC} is considered to be three-phase symmetrical. The expressions of each phase output perturbation i_p, and PCC voltage u_{PCC} are as follows

$$\begin{cases} i_{p\_a} = I_p\cos(\omega_p t + \varphi_p) \\ i_{p\_b} = I_p\cos(\omega_p t + \varphi_p - \frac{2\pi}{3}) \\ i_{p\_c} = I_p\cos(\omega_p t + \varphi_p + \frac{2\pi}{3}) \end{cases} \& \begin{cases} u_{pcc\_a} = U_0\cos(\omega_0 t) \\ u_{pcc\_b} = U_0\cos(\omega_0 t - \frac{2\pi}{3}) \\ u_{pcc\_c} = U_0\cos(\omega_0 t + \frac{2\pi}{3}) \end{cases} \tag{3}$$

where I_p, ω_p, φ_p is the amplitude, angular frequency, and initial phase of the output perturbation, U_0, ω_0, φ_0 is the amplitude, angular frequency, and initial phase of the PCC voltage. It should be noted that ω_p can be a positive number or negative number and represents the positive sequence or negative

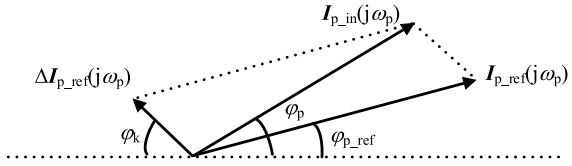

Fig. 2. The phasor diagram of the perturbation reference component $\boldsymbol{I}_{\mathrm{p\_in}}(\mathrm{j}\omega_{\mathrm{p}})$ input into the current controller in the frequency of ω_{p}.

sequence perturbation, respectively. According to (3), the AC side instantaneous power p_{ac} of IMU can be calculated as

$$\begin{aligned} p_{\mathrm{ac}} &= u_{\mathrm{pcc\_a}} i_{\mathrm{p\_a}} + u_{\mathrm{pcc\_b}} i_{\mathrm{p\_b}} + u_{\mathrm{pcc\_c}} i_{\mathrm{p\_c}} \\ &= \frac{3U_0 I_{\mathrm{p}}}{2}\{\cos((\omega_0 - \omega_{\mathrm{p}})t - \varphi_{\mathrm{p}})\} \end{aligned} \tag{4}$$

The DC side instantaneous power of IMU can be expressed as

$$\begin{aligned} p_{\mathrm{dc}} &= C\frac{du_{\mathrm{dc}}}{\mathrm{dt}} \cdot u_{\mathrm{dc}} = C\frac{d(\Delta u_{\mathrm{dc}} + U_{\mathrm{dc}})}{\mathrm{dt}} \cdot (\Delta u_{\mathrm{dc}} + U_{\mathrm{dc}}) \\ &= CU_{\mathrm{dc}}\frac{d(\Delta u_{\mathrm{dc}})}{\mathrm{dt}} \end{aligned} \tag{5}$$

where Δu_{dc} is the fluctuation component, and U_{dc} is the steady-state component and equal to the reference value of DC voltage when IMU is stable. The instantaneous power of AC side and DC side is equal,when the switching loss of bridge circuit and parasitic parameter loss of inductor are ignored. And the fluctuation component Δu_{dc} can be calculated as

$$\Delta u_{\mathrm{dc}} = \frac{3U_0 I_{\mathrm{p}}}{2CU_{\mathrm{dc}}(\omega_0 - \omega_{\mathrm{p}})}\{\sin((\omega_0 - \omega_{\mathrm{p}})t)\} \tag{6}$$

The fluctuation component Δu_{dc} is introduced to the DC voltage controller, and new fluctuation component $\Delta u'_{\mathrm{dc}}$ will be formed as

$$\begin{aligned} \Delta u'_{\mathrm{dc}} &= k_{\mathrm{pdc}}\Delta u_{\mathrm{dc}} + k_{\mathrm{idc}}\int \Delta u_{\mathrm{dc}} dt \\ &= \frac{3U_0 I_{\mathrm{p}}}{2\mathrm{C}U_{\mathrm{dc}}(\omega_0 - \omega_{\mathrm{p}})} M_{\mathrm{k}} \sin((\omega_0 - \omega_{\mathrm{p}})t + \varphi_{\mathrm{k}}) \end{aligned} \tag{7}$$

where M_{k} and φ_{k} is the amplitude gain and phase shift angle caused by DC voltage controller, and the specific expression is given by

$$\begin{cases} M_{\mathrm{k}} = \sqrt{k_{\mathrm{pdc}}^2 + (\frac{k_{\mathrm{idc}}}{\omega_0 - \omega_{\mathrm{p}}})^2} \\ \varphi_{\mathrm{k}} = \arctan(\frac{k_{\mathrm{idc}}}{(\omega_{\mathrm{p}} - \omega_0)k_{\mathrm{pdc}}}) \end{cases} \tag{8}$$

where the arctan is the abbreviation of arctangent function. The fluctuation component $\Delta u'_{\mathrm{dc}}$is regarded as d-axis component and transformed into the additional current command $\Delta i_{\mathrm{p\_ref}}$ in abc-axis, where the q-axis component is 0 and conversion angle θ_{PLL} is provided by PLL. The steps can be shown as (9), shown at the bottom of the next page. It can be seen that the additional current command $\Delta i_{\mathrm{p\_ref}}$ contains two components. One is the component $\Delta \boldsymbol{I}_{\mathrm{p\_ref}}(\mathrm{j}\omega_{\mathrm{p}})$ owned the same frequency with perturbation current command $\boldsymbol{I}_{\mathrm{p\_ref}}(\mathrm{j}\omega_{\mathrm{p}})$, and the other is the coupling component $\Delta \boldsymbol{I}_{\mathrm{p\_ref}}(\mathrm{j}2\omega_0 - \omega_{\mathrm{p}})$ with a frequency of $2\omega_0 - \omega_{\mathrm{p}}$. The phasor diagram of the actual perturbation command $\boldsymbol{I}_{\mathrm{p\_in}}(\mathrm{j}\omega_{\mathrm{p}})$ input into the current controller is shown in Fig. 2, where $\varphi_{\mathrm{p\_ref}}$ is the phase of perturbation current command $\boldsymbol{I}_{\mathrm{p\_ref}}(\mathrm{j}\omega_{\mathrm{p}})$. Obviously, the introduction of the additional current command $\Delta \boldsymbol{I}_{\mathrm{p\_ref}}(\mathrm{j}\omega_{\mathrm{p}})$ will cause the significant difference between the output perturbation $\boldsymbol{I}_{\mathrm{p}}(\mathrm{j}\omega_{\mathrm{p}})$

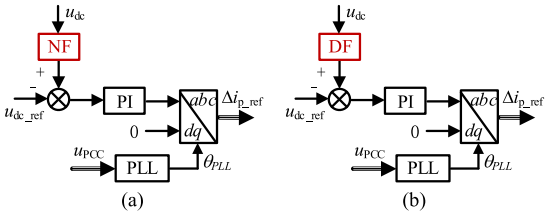

Fig. 3. The diagram of the solution of inaccurate perturbation output. (a) The single-frequency perturbation injection. (b) The multi-frequency perturbation injection.

and the perturbation current command $\boldsymbol{I}_{\mathrm{p\_ref}}(\mathrm{j}\omega_{\mathrm{p}})$, when the perturbation angular frequency ω_{p} is close to the angular frequency of the measured system ω_0 and the amplitude of $\Delta \boldsymbol{I}_{\mathrm{p\_ref}}(\mathrm{j}\omega_{\mathrm{p}})$ is considerable. Furthermore, the coupling perturbation with a frequency of $2\omega_0 - \omega_{\mathrm{p}}$, caused by coupling component $\Delta \boldsymbol{I}_{\mathrm{p\_ref}}(\mathrm{j}2\omega_0 - \omega_{\mathrm{p}})$, will also be injected into the measured system, which may increase the system burden and worsen power quality.

B. Solutions

It has been analyzed that the root cause of inaccurate perturbation output is the additional current command introduced by the DC control loop. And the problem to be solved is the perturbation injection near the fundamental frequency of measured system. Therefore, an intuitive solution is to introduce a filter to prevent the generation of corresponding additional current command. The IMU may inject single-frequency perturbation or multi-frequency perturbation into the measured system according to different measurement requirements. In this brief, the corresponding solutions are designed to accommodate both injection modes.

1) The Solution for Single-Frequency Perturbation Injection: According to the previous analysis, the voltage ripple of DC capacitor contains only one component whose frequency meets $\omega_0 - \omega_{\mathrm{p}}$, when single-frequency perturbation is injected into measured system. Thus, as shown in Fig. 3(a), a notch filter (NF) is embedded in the DC controller to filter out the fluctuation component with an angular frequency of $|\omega_0 - \omega_{\mathrm{p}}|$. The transfer function G_{NF} of the NF is given in (10).

$$G_{\mathrm{NF}}(s) = \frac{s^2 + \omega_n^2}{s^2 + \eta\omega_n s + \omega_n^2} \tag{10}$$

where ω_{n} is the notch angular frequency and η is the notch factor. The notch factor η is 0.707 to ensure the notch effect and dynamic characteristic and the ω_{n} is set as $|\omega_0 - \omega_{\mathrm{p}}|$ to corresponding voltage ripple of DC capacitor. For example, the notch angular frequency ω_{n} is set to 10π rad, when the injected perturbation is positive sequence 45Hz or 55Hz since corresponding voltage ripple of DC capacitor in 5Hz can be filtered out, and the same frequency component $\Delta \boldsymbol{I}_{\mathrm{p\_ref}}(\mathrm{j}\omega_{\mathrm{p}})$ and coupling component $\Delta \boldsymbol{I}_{\mathrm{p\_ref}}(\mathrm{j}2\omega_0 - \omega_{\mathrm{p}})$ will not be introduced into current control loop. The result is that IMU can achieve accurate perturbation output without coupling perturbation.

2) The Solution for Multi-Frequency Perturbation Injection: Multi-frequency perturbation may be injected into the measured system in the scenario, where the measurement time is high concerned. The voltage ripple of DC capacitor will contain multiple components, when the IMU is running in the multi-frequency perturbation injection mode. Suppose that

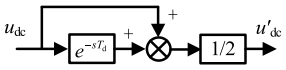

Fig. 4. The schematic diagram of the delay filter.

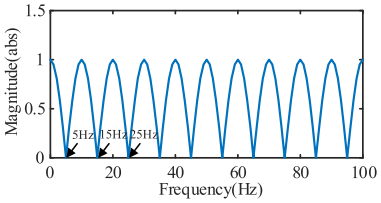

Fig. 5. The magnitude–frequency plot of $G_{DF}(s)$.

there are n components injected by IMU at one multi-frequency perturbation injection, and the frequencies are ω_{p1}, ω_{p2}, ω_{p3}, ..., and ω_{pn}. The frequencies of components in the voltage ripple of DC capacitor are $|\omega_0-\omega_{p1}|$, $|\omega_0-\omega_{p2}|$, $|\omega_0-\omega_{p3}|$, ..., and $|\omega_0-\omega_{pn}|$, respectively. To remove multi-frequency components in the voltage ripple of DC capacitor, a delay filter (DF) is embedded in the controller as shown is Fig. 3(b). The schematic diagram of the DF is shown in Fig. 4, where the output u'_{dc} is half of the sum of u_{dc} and its delayed component. The transfer function G_{DF} of the DF is given by

$$G_{DF}(s) = (1 + e^{-sT_d})/2 \tag{11}$$

where the T_d is the delay time, and it is adjusted according to the multi-frequency components to be removed. The DF can achieve 0 gain in the frequency ω_i which the following equation is satisfied.

$$\omega_i = (1 + 2i)\pi/T_d \; i = 0, \; 1, \; 2 \ldots \tag{12}$$

where i is a natural number. The magnitude–frequency plot of $G_{DF}(s)$ is shown is Fig. 5, where delay time T_d is set to 0.1s. It can be seen that the frequency points satisfied (12) can achieve 0 gain, such as 5Hz, 15Hz and 25Hz, et al. Therefore, the frequencies of components in the voltage ripple of DC capacitor is designed to fall on the frequency ω_i to achieve accurate perturbation output in the multi-frequency perturbation injection mode, which can be achieved by adjusting the frequency of the injection perturbation and the delay time T_d of DF. One example is those positive sequence components with the frequency of 35Hz, 45Hz, 55Hz, 65Hz can be injected simultaneously, when the delay time T_d is set to 0.1s.

IV. Experimental Results

The CHIL experiment was implemented to verify the effectiveness of the proposed NF-based and DF-based methods and the frame of the CHIL-based experiment system for verification is shown in Fig. 6, where the controller is implemented by TMS320F28335 to regulate the IMU and the rest of the measured system including the grid, the load, and the main

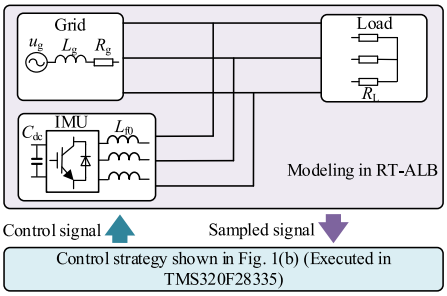

Fig. 6. The frame of the CHIL-based experiment system for verification.

TABLE I
Parameters of the Measured System

Parameters	Values	Parameters	Values
filter inductor $L_{f(I)}$/mH	5	Grid resistance R_g/Ω	1
dc voltage $U_{dc\ ref}$/V	800	Grid inductor L_g /mH	1
IMU current regulator PR	k_p=5.0, k_r=100.0	Load resistance R_L/Ω	10
IMU voltage regulator PI	k_{pdc}=0.4, k_{idc}=2.0	Delay time T_d of delay filter /s	0.1

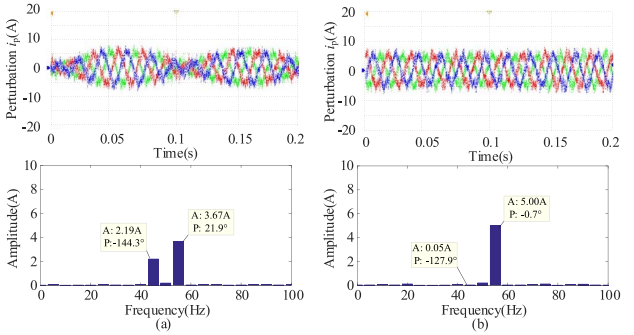

Fig. 7. The wave and FFT results of the single-frequency perturbation injection in case 1. (a) Without NF. (b) With NF.

circuit of the IMU are executed in RT-LAB. Relevant parameters of the measured system are given in Table I. Two different output mode including the single-frequency perturbation injection and the multi-frequency perturbation injection are carried out.

A. Results of the Single-Frequency Perturbation Injection Mode

*Case 1:*The IMU is controlled to inject a positive sequence perturbation, with an amplitude of 5 A, frequency of 55 Hz, and phase of 0°, into measured system. The actual injection current i_p with and without NF are shown in Fig. 7. Where the amplitude and phase of the output perturbation of the IMU without the NF are 3.67 A and 21.9° and there is a coupling perturbation (component in 45Hz) with an amplitude of 2.19 A. However, the IMU with notch can achieve accurate output perturbation whose amplitude and phase are 5.00 A and −0.7°, and the coupling perturbation is desirable.

$$\begin{bmatrix} \Delta i_{p_{R\ refa}} \\ \Delta i_{p_{R\ refb}} \\ \Delta i_{p\_refc} \end{bmatrix} = \begin{bmatrix} \cos(\omega_0 t) & -\sin(\omega_0 t) & 1 \\ \cos\left(\omega_0 t - \frac{2}{3}\pi\right) & -\sin\left(\omega_0 t - \frac{2}{3}\pi\right) & 1 \\ \cos\left(\omega_0 t + \frac{2}{3}\pi\right) & -\sin\left(\omega_0 t + \frac{2}{3}\pi\right) & 1 \end{bmatrix} \begin{bmatrix} \Delta u'_{dc} \\ 0 \\ 0 \end{bmatrix} = \frac{3U_0 I_p M_k}{4CU_{dc}(\omega_0 - \omega_p)} \begin{bmatrix} \sin\left((2\omega_0 - \omega_p)t + \varphi_k\right) - \sin\left(\omega_p t - \varphi_k\right) \\ \sin\left((2\omega_0 - \omega_p)t + \varphi_k - \frac{2}{3}\pi\right) - \sin\left(\omega_p t - \frac{2}{3}\pi - \varphi_k\right) \\ \sin\left((2\omega_0 - \omega_p)t + \varphi_k + \frac{2}{3}\pi\right) - \sin\left(\omega_p t + \frac{2}{3}\pi - \varphi_k\right) \end{bmatrix} \tag{9}$$

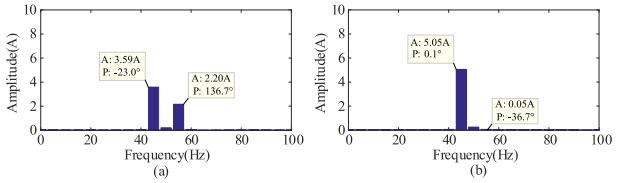

Fig. 8. FFT results of the single-frequency perturbation injection in case 2. (a) Without NF. (b) With NF.

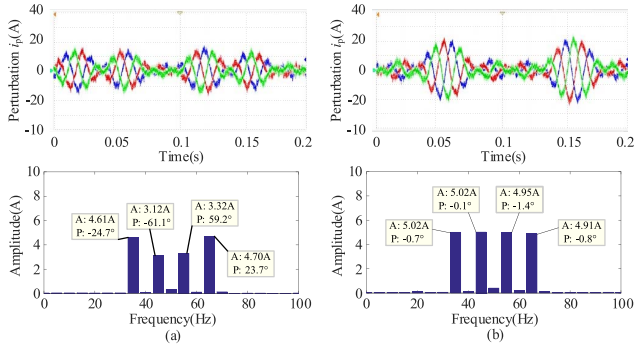

Fig. 9. The wave and FFT results of the multi-frequency perturbation injection in case 3. (a) Without DF. (b) With DF.

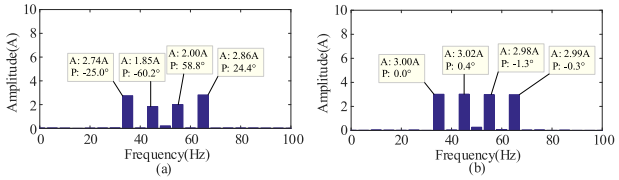

Fig. 10. FFT results of the multi-frequency perturbation injection in case 4. (a) Without DF. (b) With DF.

Case 2: In this case, the perturbation frequency is change to 45Hz and other parameters remain unchanged. The FFT results of the single-frequency perturbation injection with and without NF are shown in Fig. 8, where the effectiveness of the proposed method with NF is proved again.

B. Results of the Multi-Frequency Perturbation Injection Mode

Case 3: The IMU is controlled to realize multi-frequency perturbation injection, where the frequencies of injected components are 35 Hz, 45 Hz, 55 Hz and 65 Hz. The reference value of amplitude and phase of these components are 5 A and 0°. The actual injection current i_{p} with and without DF are shown in Fig. 9, where the amplitude and phase of the output perturbation of the IMU without the DF have certain deviations from the expected value, and the frequency component closer to the fundamental frequency has greater output error. In contrast, the IMU with the DF can achieve accurate perturbation output at all controlled frequencies.

Case 4: In this case, amplitude of these perturbations is tuned to 3A and other parameters remain unchanged. The FFT results of multi-frequency perturbation injection with and without DF are shown in Fig. 10, where the proposed method with DF achieve accurate control of multiple perturbations. It proves that a DF is expected for the IMU to achieve higher output accuracy in multi-frequency perturbation injection mode.

V. Conclusion

This brief has presented the mechanism of inaccurate perturbation output of the IMU, which are caused by additional current command from DC voltage ripple. The DF and NF based method is proposed to filter out DC voltage ripple and achieve inaccurate perturbation output in single-frequency and multi-frequency perturbation injection mode, respectively. The effectiveness of proposed solutions are proved by the CHIL-based experiment results.

References

[1] A. Akhavan, J. C. Vasquez, and J. M. Guerrero, "A robust method for controlling grid-connected inverters in weak grids," *IEEE Trans. Circuits Syst. II, Exp. Brief*, vol. 68, no. 4, pp. 1333–1337, Apr. 2021.

[2] P. Cheng, H. Kong, J. Ma, and L. Jia, "Overview of resilient traction power supply systems in railways with interconnected microgrid," *CSEE J. Power Energy Syst.*, vol. 7, no. 5, pp. 1122–1132, Sep. 2021.

[3] D. Karimipour and F. R. Salmasi, "Stability analysis of AC microgrids with constant power loads based on Popov's absolute stability criterion," *IEEE Trans. Circuits Syst. II, Exp. Brief*, vol. 62, no. 7, pp. 696–700, Jul. 2015.

[4] C. Zhang, X. Cai, A. Rygg, and M. Molinas, "Sequence domain SISO equivalent models of a grid-tied voltage source converter system for small-signal stability analysis," *IEEE Trans. Energy Convers.*, vol. 33, no. 2, pp. 741–749, Jun. 2018.

[5] M. Cespedes and J. Sun, "Adaptive control of grid-connected inverters based on online grid impedance measurements," *IEEE Trans. Sustain. Energy*, vol. 5, no. 2, pp. 516–523, Apr. 2014.

[6] W. Zhang, Y. Wen, and C. Y. Chung, "Impedance-based online estimation of nodal inertia and primary frequency regulation capability," *IEEE Trans. Power Syst.*, vol. 38, no. 3, pp. 2748–2760, May 2023, doi: 10.1109/TPWRS.2022.3186525.

[7] M. Wu, J. Li, Q. Liu, S. Yang, and M. Molinas, "Measurement of impedance-frequency property of traction network using cascaded H-bridge converters: Device design and on-site test," *IEEE Trans. Energy Convers.*, vol. 35, no. 2, pp. 746–756, Jun. 2020.

[8] P. Zhong, J. Sun, Z. Tian, P. Yu, and X. Zha, "CDSC-based adaptive impedance measurement method for grid-tied inverter system under adverse grid voltage conditions," *IEEE Trans. Ind. Electron.*, vol. 69, no. 11, pp. 11210–11220, Nov. 2022.

[9] Z. Liu, J. Liu, and Z. Liu, "Analysis, design, and implementation of impulse-injection-based online grid impedance identification with grid-tied converters," *IEEE Trans. Power Electron.*, vol. 35, no. 12, pp. 12959–12976, Dec. 2020.

[10] T. Roinila and T. Messo, "Online grid-impedance measurement using ternary-sequence injection," *IEEE Trans. Ind. Appl.*, vol. 54, no. 5, pp. 5097–5103, Sep./Oct. 2018.

[11] V. Valdivia, A. Lázaro, A. Barrado, P. Zumel, C. Fernández, and M. Sanz, "Impedance identification procedure of three-phase balanced voltage source inverters based on transient response measurements," *IEEE Trans. Power Electron.*, vol. 26, no. 12, pp. 3810–3816, Dec. 2011.

[12] H. Hu, P. Pan, Y. Song, and Z. He, "A novel controlled frequency band impedance measurement approach for single-phase railway traction power system," *IEEE Trans. Ind. Electron.*, vol. 67, no. 1, pp. 244–253, Jan. 2020.

[13] Z. Shen, M. Jaksic, P. Mattavelli, D. Boroyevich, J. Verhulst, and M. Belkhayat, "Three-phase AC system impedance measurement unit (IMU) using chirp signal injection," in *Proc. 28th Annu. IEEE Appl. Power Electron. Conf. Expo. (APEC)*, 2013, pp. 2666–2673.

[14] W. Xu, E. E. Ahmed, X. Zhang, and X. Liu, "Measurement of network harmonic impedances: Practical implementation issues and their solutions," *IEEE Trans. Power Del.*, vol. 17, no. 1, pp. 210–216, Jan. 2002.

[15] M. Li, H. Nian, B. Hu, Y. Xu, Y. Liao, and J. Yang, "An improved impedance measurement method based on multi-sine signal considering the suppression of noise interference," *IEEE Access*, vol. 9, pp. 34221–34230, 2021.

[16] M. Jakšić et al., "Medium-voltage impedance measurement unit for assessing the system stability of electric ships," *IEEE Trans. Energy Convers.*, vol. 32, no. 2, pp. 829–841, Jun. 2017.

[17] M. Petković, N. Hildebrandt, F. D. Freijedo, and D. Dujić, "Cascaded H-bridge multilevel converter for a high-power medium-voltage impedance-admittance measurement unit," in *Proc. Int. Symp. Ind. Electron. (INDEL)*, 2018, pp. 1–8.

[18] M. Jaksic, Z. Shen, I. Cvetkovic, D. Boroyevich, R. Burgos, and P. Mattavelli, "Multi-level single-phase shunt current injection converter used in small-signal dq impedance identification," in *Proc. Annu. IEEE Appl. Power Electron. Conf. Expo. (APEC)*, 2014, pp. 2775–2782.

[19] J. Zhao, M. Huang, and X. Zha, "Nonlinear analysis of PLL damping characteristics in weak-grid-tied inverters," *IEEE Trans. Circuits Syst. II, Exp. Brief*, vol. 67, no. 11, pp. 2752–2756, Nov. 2020.